Available online at www.sciencedirect.com
ScienceDirect
Journal of the European Ceramic Society 28 (2008) 2629–2637
www.elsevier.com/locate/jeurceramsoc

Analysis of the development of microscopic residual stresses on quartz particles in porcelain tile☆,☆☆

Agenor De Noni Junior[a,*], Dachamir Hotza[b], Vicente Cantavella Soler[c], Enrique Sanchez Vilches[c]

[a] *Instituto Maximiliano Gaidzinski (IMG), 88845-000 Cocal do Sul, SC, Brazil*
[b] *Universidade Federal de Santa Catarina (UFSC), 88040-900 Florianópolis, SC, Brazil*
[c] *Instituto de Tecnologia Cerámica (ITC), 12006 Castellón, Spain*

Received 3 November 2007; received in revised form 31 March 2008; accepted 12 April 2008
Available online 5 June 2008

Abstract

This paper examines the development of microscopic residual stresses on quartz particles in porcelain tile using the XRD technique. The study was conducted with a typical porcelain tile composition consisting of sodium feldspar, kaolin, and quartz, using quartzes with different particle sizes. The methodology used, based on determining the volume strain of the quartz unit cell, allowed a residual stress value equivalent to the entire particle and not just to a given crystalline plane to be obtained. The linear thermal expansion measurements indicated that, for all test compositions, the quartz in the mixture contributes to a thermal expansion coefficient comparable to the expansion of its c-lattice parameter. When this information was taken into account in the theoretical estimation of microscopic residual stress, the results were verified to be consistent with the experimental measurements.

Keywords: Firing; X-ray methods; Thermal expansion; Quartz; Porcelain tile; Tilos

1. Introduction

Porcelain tile sales have grown highly in recent years. Annual porcelain tile production currently stands at more than 6×10^8 m^2 in Europe, with turnover exceeding 6×10^9 €/annum.

Porcelain tile is a high-performing product that basically consists of an abundant glassy matrix (50–65%), quartz (10–25%), mullite (<10%), and non-fused feldspars (0–10%), and has a closed porosity of 3–7%.[1] Most of the glassy matrix comes from fusion of the feldspars, while another part stems from the clay phases that do not crystallise into mullite during firing.[2,3] Though these compositions resemble porcelain compositions,[4] the manufacturing process differs considerably, especially in the firing stage, since porcelain tile firing cycles are much faster (40–60 min) than typical porcelain firing cycles (12–24 h).

This similarity has essentially led to three theories on the strengthening mechanisms in triaxial porcelains,[4] which may be applied to porcelain tile[5]: interconnection of acicular mullite crystals; dispersion of crystalline phases that limit the critical size of the natural flaw; and matrix strengthening as a result of the difference between the linear thermal expansion coefficients of the matrix and those of the disperse crystalline phases. These mechanisms act simultaneously, and it is difficult to determine which contributes most.

In many studies on triaxial porcelains,[6–10] quartz is considered to play an important role in the resulting product properties. In porcelain tiles, this role is even more critical because quartz is the most abundant crystalline phase in the end product. On the one hand, the difference between the thermal expansion coefficients of the quartz and the matrix has a strengthening effect since it subjects the matrix to a microscopic residual compressive

☆ Based in part on the thesis submitted by A. De Noni Jr. for the Ph.D. degree in Materials Science and Engineering (PGMAT), Universidade Federal de Santa Catarina (UFSC), Brazil, 2007.

☆☆ This work was financially supported by the Brazilian Research Agency CAPES, under scholarship 2933-05-5 and co-financed by the Spanish Ministry of Industry, Tourism, and Trade for the Technology Institute Support Programme, under grant FIT-030000-2005-315/FIT-030000-2006-119.

* Corresponding author. Tel.: +55 48 3447 7736; fax: +55 48 3447 7736.
E-mail address: agenor@imgnet.org.br (A. De Noni Junior).

0955-2219/$ – see front matter © 2008 Elsevier Ltd. All rights reserved.
doi:10.1016/j.jeurceramsoc.2008.04.009

stress that originates during the cooling phase of the industrial firing cycle. Recent studies have demonstrated the existence of such residual stresses in porcelain tile.[11,12] The magnitude of these microscopic stresses produces cracks around the quartz particles, causing stress relaxation and increasing microstructural damage,[4,7,11] adversely affecting the product's mechanical behaviour.

The two simultaneous, opposing effects are a source of controversy in the literature in regard to the ultimate effect of quartz (quantity and particle size in the composition) on porcelain mechanical behaviour.[6–10] Although numerous studies have addressed this controversy in the case of porcelains, few have examined typical porcelain tile compositions and manufacturing processes.[5]

The present study analyses the state of the microscopic residual stresses on quartz particles in porcelain tiles, using quartz with different particle size distributions. The X-ray diffraction (XRD) technique was used to evaluate the stresses in order to obtain an average value for the stress on the particles, which might be compared with the theoretical calculations valid for isotropic and spherical particles. Finally, the microstructural damage associated with these stresses was observed by scanning electron microscopy (SEM).

2. Theoretical fundamentals

2.1. Microscopic residual stress

According to Selsing[13] a spherical particle of an isotropic elastic material embedded in an infinite matrix develops residual stresses in accordance with Eqs. (1) and (2).

$$\sigma_{rr} = \frac{\Delta\alpha\ \Delta T}{K_e}\left(\frac{R}{x}\right)^3, \quad x \geq R \tag{1}$$

$$\sigma_{\theta\theta} = \frac{-\sigma_{rr}}{2} \tag{2}$$

where σ_{rr} is radial stress; $\Delta\alpha$, the difference between the linear thermal expansion coefficients of the particle and the matrix; ΔT, the cooling temperature range which (in the case of a glassy matrix) is from about glass transformation temperature (T_g) to ambient temperature (T_{amb}); R, particle radius; x, the distance from the particle centre to a point in the matrix; $\sigma_{\theta\theta}$, tangential stress; K_e, a function of the modulus of elasticity (E) and Poisson's ratio (ν) of the glassy matrix (m) and of the crystalline particle (c), expressed by:

$$K_e = \frac{1+\nu_m}{2E_m} + \frac{1-2\nu_c}{E_c} \tag{3}$$

These stresses maximise at the particle–matrix interface. Radial stresses of the same magnitude as those at the interface act inside the particle.

2.2. Critical particle size

Residual stresses can cause spontaneous fracture at the interface. Ito et al.[14] proposed a model, based on fracture mechanics, which might be able to predict a critical particle diameter (d_c) above which fracture would occur:

$$d_c = \frac{1}{0.15\ \sin(\omega(2-\sin\omega))}\frac{\gamma_i K_e}{(\Delta\alpha\,\Delta T)^2} \tag{4}$$

where γ_i is matrix fracture energy; ω, the ratio of semispherical crack size to particle diameter; $\omega \sim 0.3$ would correspond to a typical value calculated by Ito et al.[14]

2.3. Microscopic stress measurement by X-ray diffraction

The X-ray diffraction technique for measuring residual stresses uses the crystal planes as an absolute strain gauge.[15] When a material is subjected to stress, the crystal plane spacing changes and the diffraction peak shifts, as expressed by Eq. (5).

$$\varepsilon_{hkl} = -\frac{1}{2}\ \cot(\theta)\Delta(2\theta) = \frac{d^{ti}_{hkl} - d^0_{hkl}}{d^0_{hkl}} \tag{5}$$

where $\Delta(\theta)$ is the diffraction peak shift; θ, the diffraction angle of the unstressed material; d^{ti}_{hkl}, the interplanar spacing of the stressed material; d^0_{hkl}, the interplanar spacing of the unstressed material.

Once the displacement of a given plane is known, Hooke's law can be applied to determine the stress acting upon it. Eq. (1) can be applied for each plane, when plane properties are known, in order to compare the theoretical values with the experimental data.[16] However, this information cannot be considered representative of the stress state of the entire particle, especially in particles that behave anisotropically, such as quartz particles.

2.4. Microscopic residual stresses on quartz in triaxial porcelains

Investigations of triaxial porcelains on this subject[6,9,17] have attempted to correlate displacements of quartz plane [1 1 2] or [2 1 1] with mechanical properties. When the theoretical values of the displacements are compared with the experimental ones, partial stress relief is observed, but a strengthening effect may also be expected owing to the remaining stresses. However, quartz particles are usually partly dissolved,[9,18,19,20] so that they can increase the interplanar displacement when they develop an interphase with a glassy phase that is richer in amorphous silica and, hence, has a smaller thermal expansion than the predominant glassy matrix.

Data published by Hamano et al.[9] show how partial dissolution of the quartz particles affects the displacement of the crystal planes. These authors prepared triaxial porcelain test pieces (50% kaolin, 25% feldspar, 25% quartz), varying quartz particle size ($D_{50} \sim 2$, 7, 15, 25, 35 μm, with very narrow amplitudes because of preparation by elutriation) and firing temperature (between 1200 and 1400 °C, in steps of 50 °C, and 1-h hold at peak temperature). They then determined the remaining quantity of quartz, and compared the intensities of the diffraction peaks with those of the green material (I/I_0) (values between 0.10 and 0.84), and the interplanar spacing of plane [2 1 1].

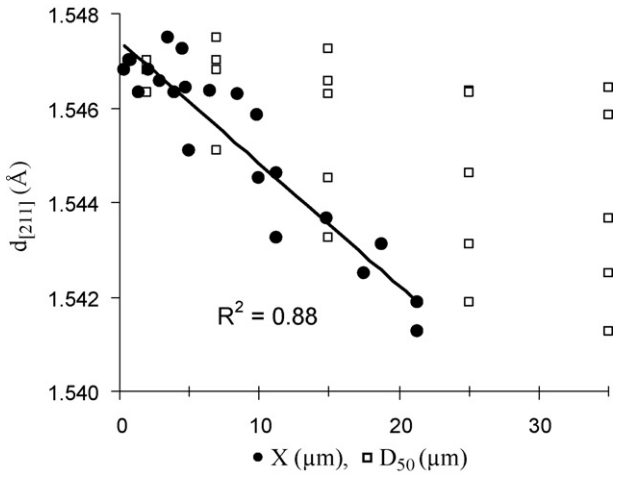

Fig. 1. Variation of quartz interplanar spacing ($d_{[2\,1\,1]}$) with particle initial mean diameter (D_{50}) and the product of D_{50} and I/I_0 (X).

The Hamano data[9] have been used for the graph shown in Fig. 1, which relates the quartz interplanar spacing to initial mean particle diameter, D_{50}, and to a variable defined as the product of the remaining quartz quantity (I/I_0) and initial mean particle diameter (D_{50}), expressed by the following equation:

$$X = D_{50}\frac{I}{I_0} \tag{6}$$

These results indicate that quartz particles of the same initial size may display different interplanar distances, depending on the particle state of dissolution. As a quartz particle dissolves, the interphase becomes richer in silica and the remaining quartz exhibits a larger interplanar spacing. The variable X represents a semi-quantitative approximation of remaining quartz particle size. Though residual stress is not a function of particle diameter (Eq. (1)), good correlation is observed with regard to X because of the changes in the nature of the interphase (mainly the thermal expansion coefficient and thickness of the layer that forms around the particles with respect to particle size).

3. Calculation method for estimating equivalent isotropic microscopic residual stress for anisotropic particles

Equivalent isotropic microscopic residual stress was estimated using the diffraction peak values to calculate stressed unit cell volume. For the hexagonal system, volume may be determined from the a- and c-lattice parameters with Eq. (7).

$$V = 0.866a^2c \tag{7}$$

The parameters may be calculated from Eq. (8), which describes the geometric relations between the lattice parameters and the crystal plane spacings[21,22]:

$$\frac{1}{d^2_{[hkl]}} = \frac{4}{3}\left(\frac{h^2+hk+k^2}{a^2}\right) + \frac{l^2}{c^2} \tag{8}$$

The interplanar spacing may be calculated by XRD, applying Bragg's law. This requires using the information on two planes to establish a system of two equations and two unknowns. For quartz the most appropriate planes are [1 1 2] and [2 1 1] since they appear at larger angles, which minimise the experimental error, as Eq. (5) indicates. Though their intensities are low, they suffice to determine plane positions.

Once the unit cell volume has been calculated, the resulting expansion or shrinkage (ε_V) due to residual stresses may be determined from Eq. (9):

$$\varepsilon_V = \frac{V - V_0}{V_0} \tag{9}$$

where V_0 is the volume of the material's characteristic unit cell. The cell volume calculated from Eq. (1) can be rewritten as follows:

$$V = 0.866\ a_0^2(1+\varepsilon_a)^2c_0(1+\varepsilon_c) = V_0(1+\varepsilon_a)^2(1+\varepsilon_c) \tag{10}$$

Since quartz displays anisotropic behaviour, the strains at a and c differ. The equivalent linear strain 'ε' is defined as the isotropic strain that would lead to the same variation in volume as Eq. (10)

$$V = V_0(1+\varepsilon_a)^2(1+\varepsilon_c) = V_0(1+\varepsilon)^3 \tag{11}$$

This procedure is the same as that used to calculate the equivalent linear thermal expansion coefficient of a polycrystalline anisotropic material. Combining Eqs. (9) and (11) allows determination of the equivalent linear strain associated with the particle:

$$\varepsilon = (1+\varepsilon_V)^{1/3} - 1 \tag{12}$$

The equivalent isotropic stress may be estimated by applying Hooke's law, as follows:

$$\sigma_r = \varepsilon E \approx \sigma_{rr} \tag{13}$$

4. Experimental procedure

The tests were carried out with a porcelain tile composition consisting of approximately 50% albite, 30% kaolinite, and 20% quartz, only varying quartz particle size. A floated sodium feldspar (Kaltun) and the Super Standard Porcelain kaolin (Imerys) were used, respectively, as a source of albite and kaolinite. Four types of quartz were used: SE500 (Q1), SE100 (Q2), SE12 (Q3), and SE8 (Q4) (Sibelco) giving rise to the corresponding compositions PQ1, PQ2, PQ3 and PQ4, respectively. The chemical compositions are detailed in Table 1. The particle size distributions have been plotted in Fig. 2. However, the

Table 1
Chemical composition of the materials used (% by weight)

	Feldspar	Kaolin	Quartz
SiO_2	68	47	98.9
Al_2O_3	19.2	38	0.51
Na_2O	10.9	0.15	0.01
K_2O	0.23	0.80	0.06
CaO	1.1	0.10	0.03
Others	0.34	0.64	0.11
LOI	0.14	13.0	0.27

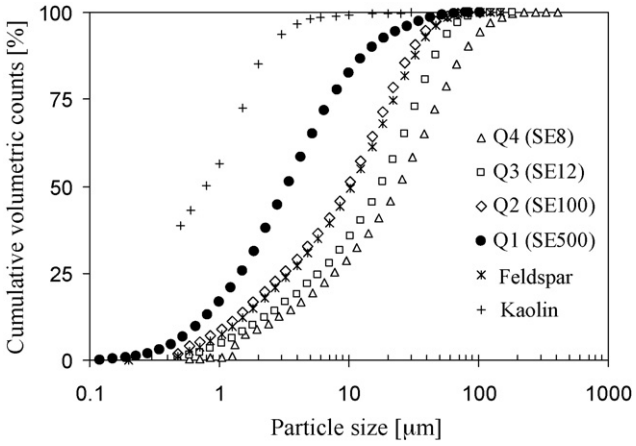

Fig. 2. Particle size distribution of the materials used.

quartz particle size distributions in the starting mixtures differed slightly from those of the quartz used in each case, since about 17% of the quartz in the composition came from the feldspar.

The test mixtures (PQ1, PQ2, PQ3, and PQ4) were proportioned, homogenised by wet milling for 45 min, and then spray dried. Mixture PQ2 is closest to a standard industrial composition, so that the test compositions together fully encompass the compositional range found in industrial practice. Test pieces of 80 mm × 20 mm × 7 mm were formed at a pressing pressure of 45 MPa and moisture content of 5.5% (dry basis). The pieces were dried in an oven at 110 °C and then fired in an electric kiln. The heating cycle used was as follows: heating from 25 to 500 °C at 70 °C/min and from 500 to 1230 °C at 25 °C/min, with a 6-min hold at peak temperature followed by natural cooling in the kiln. The peak temperature used (1230 °C except for PQ1) corresponded to that at which the sintered pieces achieved maximum density (measured by the Archimedes method). The peak temperature used for composition PQ1 (finest quartz) was 1220 °C, in order to maintain the maximum density condition.

The fired materials were powdered to determine their mineralogical composition by the Rietveld method,[23] using fluorite as an internal standard. To determine the strains on lattice parameters of quartz particles, the diffraction peak displacements for planes [1 1 2] and [2 1 1] were measured directly on the surfaces of test pieces without any surface treatment and any particular orientation. A diffractometer (Bruker AXS, D8 advance), with the following experimental conditions was used: radiation K($\alpha1+\alpha2$)Cu, step size of 0.01°, scan time of 1 s/step from 10° to 70° (2θ), and 1976-NIST corundum as internal standard. The linear thermal expansion curves of two test pieces made from each mixture were determined between 100 and 950 °C with a dilatometer (Netzsch DIL 402C) at a heating rate of 10 °C/min. Finally, polished cross-sections of some test pieces were observed by SEM.

Table 2
Final mineralogical composition of the test mixtures and conversion with respect to the unfired starting mixture (η)

	Glass	Albite		Quartz		Mullite	
	ϕ_{Vi}	ϕ_A	η	ϕ_Q	η	ϕ_M	η
PQ1	0.66	0.07	0.14	0.16	0.82	0.114	0.88
PQ2	0.67	0.04	0.08	0.18	0.91	0.107	0.83
PQ3	0.65	0.04	0.08	0.20	1.0	0.106	0.83
PQ4	0.65	0.04	0.08	0.20	1.0	0.110	0.88
Error	0.02	0.005		0.01		0.01	

Table 3
Quartz crystal strains and equivalent isotropic stresses in the fired pieces obtained from the test mixtures

	$d^{ti}_{1\,1\,2}$ (Å)	$d^{ti}_{2\,1\,1}$ (Å)	ε_a ($\times10^3$)	ε_c ($\times10^3$)	ε ($\times10^3$)	σ_r (MPa)
PQ1	1.8250	1.5500	5.899	1.512	4.434	346
PQ2	1.8229	1.5477	4.290	0.879	3.152	246
PQ3	1.8227	1.5460	2.969	2.304	2.747	214
PQ4	1.8201	1.5435	1.300	1.180	1.260	98

5. Results and discussion

5.1. Mineralogical composition of the fired product

The mineralogical compositions obtained (expressed as volume fraction, ϕ) and the relation between the final mass and the initial mass of each component (η), excluding loss on ignition (LOI), are presented in Table 2. In regard to mullite, η represents the relation between the formed quantity and the quantity that could theoretically form from kaolinite, considering primary mullite ($2Al_2O_3{\cdot}SiO_2$) according to the suggestion of Lee et al.,[24] assuming alumina to be the limiting reactant.

It was observed that the end product still contained albite that had not fully fused, owing to the short residence time at peak firing temperature, even though firing had occurred at 1230 °C. Since composition PQ1 was the only composition fired at 1220 °C, a greater quantity of residual albite was observed. However, in this composition almost 20% of the quartz had dissolved because of the smaller quartz particle size. As quartz particle size increased, particle dissolution decreased, dissolution being negligible for the quartz in mixtures PQ3 and PQ4. The quantity of mullite that formed was practically the same for the four studied compositions, with a conversion of about 85%.

5.2. Microscopic residual stress on quartz particles

Table 3 presents the data obtained for the interplanar spacings and quartz unit cell strains, in addition to the equivalent isotropic stress, Eq. (13), for the fired pieces made from the test mixtures.

It was observed, first, that the residual stress values decreased as quartz particle size increased, owing to stress relaxation in the particles with the largest diameter. If no stress relaxation occurred, stresses of about 580 MPa would be expected according to Eq. (1) (assuming: $E_c = 78$ GPa,[7] $E_m = 70$ GPa,[25] $\nu_c = \nu_m = 0.2$,[7] $\Delta T = 730$ °C,[7,20] $\alpha_{c(20–750\,^\circ C)} = 2.03 \times 10^{-5}\,^\circ C^{-1}$,[26] $\alpha_{m(20–750\,^\circ C)} = 7.4 \times 10^{-6}\,^\circ C^{-1}$).[27] Under these conditions, the critical diameter foreseen by Eq. (4) (assuming $\gamma_i = 3.5$ J/m^2) would be about 10 μm. This suggests that particles with a diameter >10 μm would be completely detached

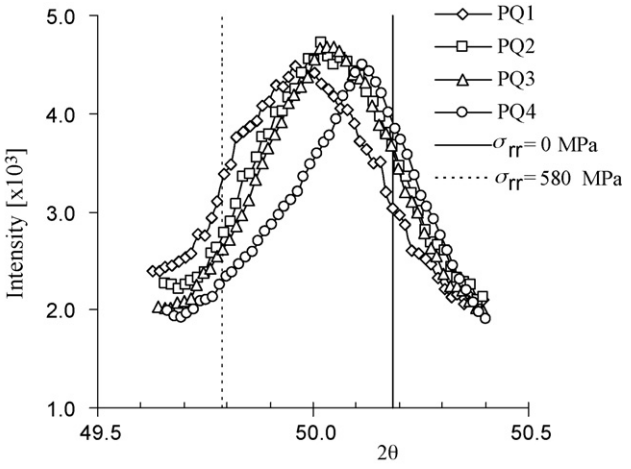

Fig. 3. Quartz diffraction peaks of the fired test pieces obtained from the studied compositions (plane [1 1 2]).

from the matrix ($\sigma_{rr} = 0$), whereas those with a diameter <10 μm would display stress of approximately 580 MPa. Although this hypothesis partly explains the observed trend, in actual fact the phenomena are more complex. Many particles with that level of stress would probably be internally fractured,[17] with the ensuing partial stress relaxation. Fig. 3 shows the diffraction peaks for quartz plane [1 1 2], the solid line representing the diffraction angle for the unstressed material and the dotted line the position that might be expected with stresses of 580 MPa. The shape of the diffraction peaks suggests that they are not formed by overlapping peaks of two types of particles: $\sigma_r = 580$ MPa and $\sigma_r = 0$, but that there are probably partly detached or broken particles with intermediate stresses, this being possibly confirmed by the diffraction peak broadening.

The smallest particles, which exhibit advanced states of dissolution, display an interphase with a glassy phase rich in amorphous silica (smaller α), which contributes to a higher stress level. This contribution to the residual stress value in test piece PQ1 is probably more significant than the fact that it has a smaller quantity of particles below the critical size.

5.3. Origin of microscopic stresses: analysis based on linear thermal expansion

In order to better understand the origin of the microscopic residual stresses on quartz particles, experimental verifications were carried out on the coefficients of linear thermal expansion of the fired test pieces prepared from the test mixtures. The results were used to estimate the contribution by the quartz particles and to determine the temperature at which microscopic stresses began to occur. Finally, the stresses were theoretically calculated from Eq. (1) and the values compared with the experimental data.

5.3.1. Coefficient of linear thermal expansion of the fired pieces obtained from the test mixtures

The results of the coefficients of linear thermal expansion of the fired pieces are plotted as a function of temperature in Fig. 4. These coefficients have been calculated starting from 100 °C, in steps of 50 °C ($\Delta T = T2 - T1$), from the slope of the thermal expansion curve. For temperatures above 500 °C, ΔT was lowered to 25 °C in order not to mask the large dimensional changes caused by the allotropic transformation of quartz. The thermal expansion curve for composition PQ2 has been plotted on the secondary axis.

In all cases α increases with temperature, peaking at ~575 °C owing to the allotropic change of quartz. Such behaviour is characteristic of quartz-containing compositions. Since test piece PQ1 contains less residual quartz, the observed peak is lower than the others. Since β-quartz practically does not expand, a pronounced drop in α values is observed after the allotropic change, the resulting values being even lower than those obtained between 100 and 500 °C. The thermal expansion curve of composition PQ2 reflects both the region of the allotropic change of quartz (~575 °C[26]) and the glass transition (T_g) region of the albite glass (~815 °C[27]). It also shows that at about 750 °C, the thermal expansion coefficient of the material begins to increase. This point approximately indicates the lower annealing temperature of the glassy phase, in addition to the temperature at which the expansion of the material is basically determined by expansion of the glassy matrix, since the existing crystalline phases start to expand more freely without greatly altering the expansion of the whole piece. On the other hand, it is at this temperature during cooling that the microscopic residual stresses between the crystalline particles and the glassy matrix begin to develop.

5.3.2. Estimation of the quartz coefficient of linear thermal expansion

The coefficient of thermal expansion is often an additive property in relation to the mixture constituents, so that α may be written as follows:

$$\bar{\alpha}_{T1-T2} = \sum_i \alpha_{i(T1-T2)}\phi_i \quad (14)$$

where $\alpha_{i(T1-T2)}$ are the values of each constituent's thermal expansion coefficients between $T1$ and $T2$, and ϕ_i their volume fraction.

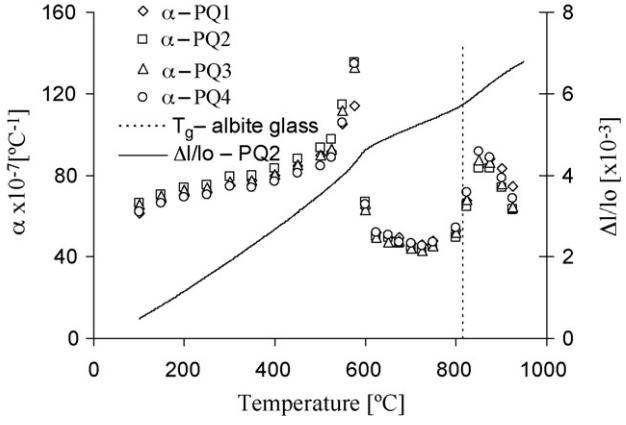

Fig. 4. Coefficients of thermal expansion of the fired pieces obtained from the test mixtures, and thermal expansion curve for composition PQ2.

Table 4
Coefficients of thermal expansion of the system constituents

Constituent	α_i (100–700) ($\times 10^{-7}\,^{\circ}C^{-1}$)
Albite[28]	75.3
Albite glass[27]	74
Mullite[29]	56.2
Kaolin glass[25]	14
Amorphous silica	5.5

As Table 2 showed, the resulting system consists of mullite, quartz, unmelted feldspar, and glassy phase. The glassy phase largely consists of glass from albite, in addition to a small portion of amorphous phase from kaolin that did not crystallise as mullite (composed by SiO_2 and Al_2O_3), and a small quantity of amorphous silica from quartz dissolution. Since firing is very rapid (fast heating rate and 6-min hold at peak temperature), there is insufficient time to develop a uniform glassy phase composition. Thus, the existence of three different glassy phases (albite glass, kaolin glass, and amorphous silica) has been taken into account in the calculation of the thermal expansion coefficient. The advantage of this approach is that, since the thermal expansion coefficients of albite glass and amorphous silica are known, it is only necessary to estimate the value of α for part of the glassy phase. The amount of each glassy phase can be then calculated from the data presented in Table 2, the start formulation and the chemical composition of each crystalline phase. The values of the thermal expansion coefficients of the materials in the system are given in Table 4. Although this system has many parameters they are all known data, either theoretically or experimentally. Therefore, the quartz linear thermal coefficient is the unique unknown parameter, and once it has been calculated, it can be compared with experimental data as well.[26]

The data in Fig. 2 and in Table 4 allowed determination of the quartz coefficient of linear thermal expansion for each temperature step ($\Delta T \sim 50\,^{\circ}C$) between 100 and 750 °C. The experimental linear thermal expansion curve for the quartz in the mixtures can thus be reconstructed using Eq. (15), to permit a direct comparative analysis with the theoretical curve.[26] The results are shown together with the linear thermal expansion curves of polycrystalline quartz and the respective quartz *a*- and *c*-lattice parameters, for comparative purposes, in Fig. 5.

$$\left.\frac{\Delta l}{l_o}\right|_{T_{n+1}} = \left.\frac{\Delta l}{l_o}\right|_{T_0} + \sum_{k=0}^{n} \bar{\alpha}_{(T_k - T_{k+1})}(T_{k+1} - T_k) \quad (15)$$

These results show that the quartz present in the porcelain tiles contributes a coefficient of linear thermal expansion that corresponds to the coefficient of the *c*-lattice parameter. This phenomenon is probably related to the microscopic stress relaxation that causes break-up of the contact with the glassy matrix. Estimation of the critical diameter, Eq. (4), corresponding to parameters *a* and *c*, gives $d_c(a) = 6\,\mu m$ and $d_c(c) = 44\,\mu m$, respectively. These values indicate that there may be a partial, oriented quartz particle detachment process owing to the anisotropic behaviour of the two lattice parameters. Ohya et al.[30] also suggest that anisotropic behaviour may determine oriented detachments or fractures. Most quartz particles in quartzes

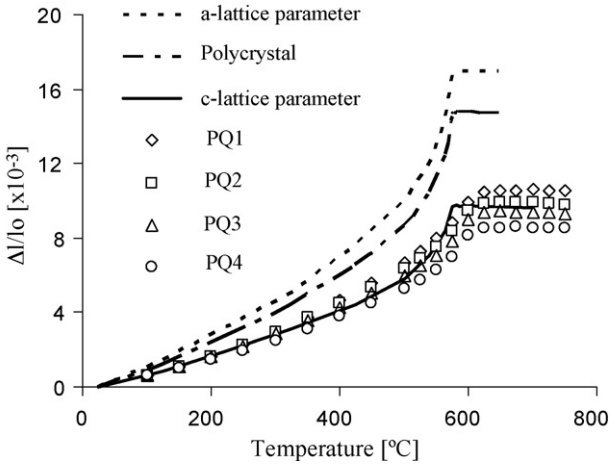

Fig. 5. Linear thermal expansion curves of the quartz in the fired pieces obtained from the test mixtures together with that of the polycrystalline quartz and the quartz *a*- and *c*-lattice parameters.[24]

Q2, Q3, and Q4 are between 6 and 44 μm in size. However, in sample PQ4 about 30% of the quartz particles are larger than 44 μm, which would explain the smaller quartz thermal expansion in composition PQ4, since these particles (>44 μm) would be completely detached from the matrix. For smaller particles, the phenomenon is more complex. In quartz Q1, which has the finest quartz particles, about 70% of the quartz particles are below 6 μm; nevertheless the thermal expansion of this quartz still exhibits the same trend as the other quartzes, though it is slightly higher. The reason for this behaviour is, first, that these small particles have an interphase with a glassy phase that is richer in silica (as a result of the dissolution process), so that the critical size for the *a*-lattice parameter becomes even smaller. Secondly, the particles that are smaller than the critical size may be fractured because, since they are not detached from the glassy matrix, the microscopic stress might exceed the fracture stress of the quartz.

5.3.3. *Theoretical calculation of microscopic residual stress*

In accordance with the results of the foregoing section, Eq. (1) can be used again to estimate the microscopic residual stress on the quartz particles, in this case, however, using the coefficient of linear thermal expansion for the quartz estimated from the experimental data in the cooling range, which was also observed experimentally. The results are presented in Table 5, together with the error in relation to the experimental data given in Table 3 (Er), calculated from Eq. (16)

$$\mathrm{Er} = \sigma_{rr,theo} - \sigma_{r,exp} \quad (16)$$

Table 5
Theoretical values of the microscopic residual stress on the quartz particles and error against the experimental measurements

	σ_{rr} (MPa)	Er (MPa)
PQ1	318	−28
PQ2	272	+27
PQ3	241	+27
PQ4	193	+95

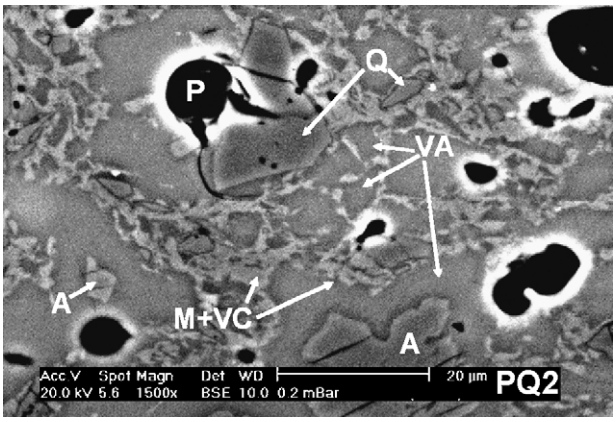

Fig. 6. Micrograph of a sintered test piece made from mixture PQ2: porosity (P), quartz (Q), albite (A), albite glass (VA), primary mullite (M), kaolin glass (VC).

The theoretical equation, Eq. (1), is defined for an infinite matrix ($\phi \rightarrow 0$). However, the studied mixtures exhibit values of $\phi \approx 0.2$. The theoretical values may therefore be expected lie slightly higher than the experimental ones (positive errors). This explains the deviation displayed by compositions PQ2 and PQ3 from the experimental errors. In addition, the consistency between the theoretical and the experimental values is related to the fact that these mixtures contain a larger quantity of particles below the critical size, d_c, related to the c-lattice parameter, estimated at ~44 μm. As a result, composition PQ4 presents a larger error, since it contains many more particles above the critical size. In addition, the results for mixture PQ1 highlight, once again, the influence that the silica-rich interphase has on the state of the stresses on the smallest particles, since higher experimental values than expected were obtained.

5.4. Analysis of the formed microstructures

Fig. 6 shows the micrograph of composition PQ2 which, as indicated, is closest to that of an industrial porcelain tile. All system features are relatively identifiable: closed porosity (P), quartz particles (Q), albite particles (A), albite glass (VA), primary mullite (M), and kaolin glass (VC). At these levels, primary mullite cannot be distinguished from the remaining kaolin glass. These two constituents share the same location because the kaolin (the constituent with the smallest particle size, which contributes plasticity to the green material) lodges between the albite and the quartz particles. These regions can be identified by visualising the limits of the positions where the glassy matrix from the albite (VA) is located. During the rapid firing cycles there is no time for the kaolin glass to diffuse through the matrix. EDX analysis suggests a Si/Al ratio comparable to that of metakaolin.[24] The albite glass regions, however, retain the original identity of the precursor particles. The remaining albite particles also preserve the identity of the original particles.

It may be further noted that the observable fractures in quartz particles beyond a certain size are mainly due to the polishing process to which the samples were subjected. Some of the remaining albite particles are also observed to be broken, even without the development of any appreciable residual stress (<5 MPa, Eq. (1)). However, it is easier to break an already stressed particle like the quartz particles, than unstressed particles. Microstructural damage at interphase levels (i.e. peripheral

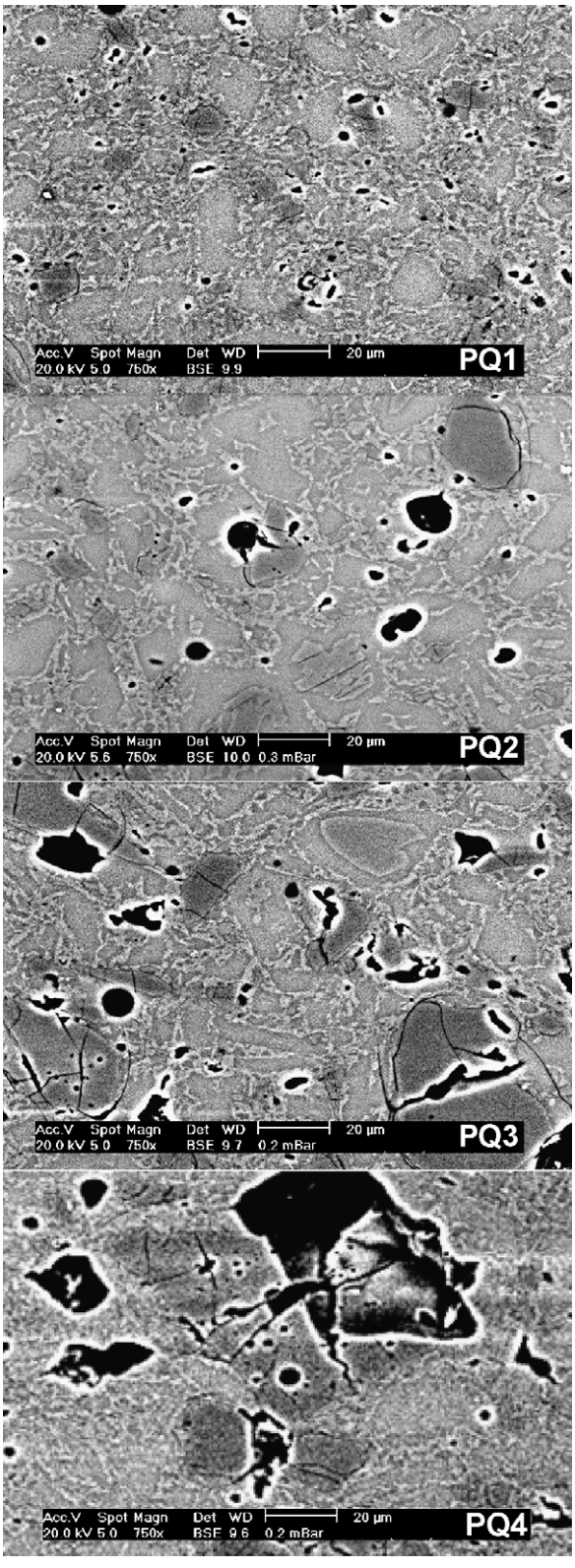

Fig. 7. Micrographs of test pieces obtained from the studied mixtures.

cracks) is caused by high stresses between the quartz and the matrix. What is observed, however, is an effect maximised by the polishing process. In this case, no peripheral cracks are observed around the remaining albite particles.

The foregoing discussion is applicable to the sequence of micrographs shown in Fig. 7, with a magnification of 750×, for all compositions: PQ1, PQ2, PQ3, and PQ4. The most noteworthy differences between these compositions relate to: (1) pore size distribution, the pores being smaller and more numerous as quartz particle size decreases and (2) the greater dispersion of the mullite crystals associated with the larger surface provided by the quartz as quartz particle size decreases. These effects are clearly distinguishable, especially when PQ1 is compared with the other compositions. As quartz particle size increases, more peripheral cracks, more transgranular fractures, and (in more extreme cases such as PQ4) completely detached or pulled-out particles may be observed.

6. Conclusions

The residual stress on quartz particles in porcelain tiles has been measured using X-ray diffraction. The method applied to quantify these stresses uses information from the displacement of two families of crystalline planes to obtain a virtually isotropic stress state for a system of anisotropic particles. This is found to be more robust when it comes to interpreting the results, particularly for such a complex system as that of porcelain tile in which the quartz particles are dispersed in a glassy matrix.

Microstructural observation shows that porcelain tile, due to its rapid firing cycle, maintains a strong identity in regard to particle packing and densification. Moreover, this is a system in which the existing glassy phases practically do not diffuse into each other, a fact that needs to be taken into account in the estimation of the quartz coefficient of linear thermal expansion.

The quartz in sintered porcelain tile displays a coefficient of linear thermal expansion equivalent to the c-lattice parameter, which is lower than the coefficient attributed to polycrystalline quartz. When this information is taken into account in the theoretical calculation of residual stress, the results display a clear consistency with the experimentally determined values. However, in the cases in which the values deviated more, this was due to two different factors: (1) the advanced state of dissolution of the smaller quartz particles, which modified the nature of the particle–matrix interphase considered in the calculation and (2) the quartz particle size distributions that contained a large fraction above the critical size for *c*-lattice parameter (estimated at about 44 μm). These results indicate that anisotropic behaviour determines quartz particle detachment from the glassy matrix.

Acknowledgements

The authors wish to thank the staff at the Instituto de Tecnología Cerámica (ITC), Spain; the Coordination for the Improvement of Higher Education Personnel (CAPES), Brazil; and the Instituto Maximiliano Gaidzinski (IMG), Brazil. The authors also thank the Spanish Ministry of Industry, Tourism, and Trade for co-financing the Technology Institute Support Programme (FIT-030000-2005-315/FIT-030000-2006-119).

References

1. Sánchez, E., Orts, M. J., Ten, J. G. and Cantavella, V., Porcelain tile composition: effect on phase formation and end products. *Am. Ceram. Soc. Bull.*, 2001, **80**, 43–49.
2. Manfredini, T., Pellacani, G. C. and Romagnoli, M., Porcelainized stoneware tile. *Am. Ceram. Soc. Bull.*, 1995, **74**, 76–79.
3. Romero, M., Marquez, J. M. and Rincón, J. M., Kinetic of mullite formation from a porcelain stoneware body for tiles production. *J. Eur. Ceram. Soc.*, 2006, **26**, 1647–1652.
4. Senapati, U. and Carty, W. M., Porcelain-raw materials, processing, phase evolution, and mechanical behavior. *J. Am. Ceram. Soc.*, 1998, **81**, 3–20.
5. Cavalcante, P. M. T., Dondi, M., Ercolani, G., Guarini, G., Melandri, C., Raimondo, M. and Almendra, E. R., The influence of microstructure on the performance of white porcelain stoneware. *Ceram. Int.*, 2004, **30**, 953–963.
6. Stathis, G., Ekonomakou, A., Stournaras, C. J. and Ftikos, C., Effect of firing conditions, filler grain size and quartz content on bending strength and physical properties of sanitaryware porcelain. *J. Eur. Ceram. Soc.*, 2004, **24**, 2357–2366.
7. Bragança, S. R., Bergmann, C. P. and Hübner, H., Effect of quartz particle size on the strength of triaxial porcelain. *J. Eur. Ceram. Soc.*, 2006, **26**, 3761–3768.
8. Hamano, K., Wu, Y. H., Nakagawa, Z. and Hasegawa, M., Effect of coarse quartz grain on mechanical strength of porcelain body. *J. Ceram. Soc. Jpn. Int. Ed.*, 1991, **99**, 1070–1073.
9. Hamano, K., Wu, Y. H., Nakagawa, Z. and Hasegawa, M., Effect of grain size of quartz on mechanical strength of porcelain bodies. *J. Ceram. Soc. Jpn. Int. Ed.*, 1991, **99**, 149–153.
10. Warshaw, S. I. and Seider, R. J., Comparison of strength of triaxial porcelains containing alumina and silica. *J. Am. Ceram. Soc.*, 1967, **50**, 337–342.
11. De Noni Jr., A., Hotza, D., Cantavella, V. and Sanchez, E., Influencia del enfriamiento de la etapa de cocción sobre las propiedades mecánicas del gres porcelánico. *Bol. Soc. Esp. Ceram. Vidrio*, 2007, **46**, 163–170.
12. De Noni Jr., A., Hotza, D., Cantavella, V. and Sanchez, E., Influence of macroscopic residual stresses on the mechanical behavior and microstructure of porcelain tile. *J. Eur. Ceram. Soc.*, 2008, **28**, 2463–2469.
13. Selsing, J., Internal stress in ceramic. *J. Am. Ceram. Soc.*, 1961, **44**, 419–425.
14. Ito, Y. M., Rosenblatt, M., Cheng, L. Y., Lange, F. F. and Evans, A. G., Cracking in particulate composites due to thermalmechanical stress. *Int. J. Fract.*, 1981, **17**, 483–491.
15. Lu, J., *Handbook of Measurement of Residual Stress*. Fairmont Press, Lilburn, 1996.
16. Mastelaro, V. R. and Zanotto, E., Anisotropic residual stress in partially crystallized Li_2O–$2SiO_2$ glass–ceramics. *J. Non-Cryst. Solids*, 1999, **247**, 79–86.
17. Carty, W. M. and Pinto, B. M., Effect of filler size on the strength of porcelain bodies. *Ceram. Eng. Sci. Proc.*, 2002, **23**, 95–105.
18. Kobayashi, Y., Ohira, O., Ohashi, Y. and Kato, E., Effect of firing temperature on bending strength of porcelains for tableware. *J. Am. Ceram. Soc.*, 1992, **75**, 1801–1806.
19. Iqbal, Y. and Lee, W. E., Fired porcelain microstructures revisited. *J. Am. Ceram. Soc.*, 1999, **82**, 3584–3590.
20. Zsolnay, L. M., Mechanical strength of porcelain. *J. Am. Ceram. Soc.*, 1957, **40**, 299–306.
21. Cullity, B. D. and Stock, S. R., *Elements of X-ray Diffraction*. Prentice-Hall, New Jersey, 2001.
22. Cucka, P. and Oliva, R. F., X-ray measurement of strain in quartz particles of whiteware bodies. *J. Am. Ceram. Soc.*, 1968, **51**, 458–464.
23. Young, R. A., *The Rietveld Method*. University Press, Oxford, 1996.

24. Lee, W. E., Souza, G. P., McConville, C. J., Tarvornpanich, T. and Iqbal, Y., Mullite formation in clays and clay-derived vitreous ceramics. *J. Eur. Ceram. Soc.*, 2008, **28**, 465–471.
25. Navarro, J. M. F., *El vidrio, constitución, fabricación y propiedades*. CSIC, Madrid, 2003.
26. Kihara, K., An X-ray study of the temperature dependence of the quartz structure. *Eur. J. Miner.*, 1990, **2**, 63–77.
27. Vergano, P. J., Hill, D. C. and Uhlmann, D. R., Thermal expansion of feldspar glasses. *J. Am. Ceram. Soc.*, 1967, **50**, 59–60.
28. Ahrens, T. J., *Mineral Physics and Crystallography: A Handbook of Physical Constants*. American Geophysical Union, Washington, D.C., 1995.
29. Schneider, H., Schreuer, J. and Hildmann, B., Structure and properties of mullite: a review. *J. Eur. Ceram. Soc.*, 2008, **28**, 329–344.
30. Ohya, Y., Takahashi, Y., Murata, M., Nakagawa, Z. and Hamano, K., Acoustic emission from a porcelain body during cooling. *J. Am. Ceram. Soc.*, 1999, **82**, 445–448.